Influence of the High Arctic Igneous Province on the Cenomanian/Turonian Boundary Interval, Sverdrup Basin, High Canadian Arctic

Claudia J. Schröder-Adams[1], Jens O. Herrle[2], David Selby[3,4], Alex Quesnel[1], Gregory Froude[1]

[1]Department of Earth Sciences, Carleton University, Ottawa, Ontario, K1S 5B6, Canada

[2]Institute of Geosciences, Altenhoeferallee 1, Goethe-University Frankfurt, Biodiversity and Climate Research Centre (BIK-F), D-60438 Frankfurt am Main, Germany

[3]Department of Earth Sciences, Durham University, DH1 3LE, Durham, United Kingdom

[4]State Key Laboratory of Geological Processes and Mineral Resources, School of Earth Resources, China University of Geosciences Wuhan, Wuhan, China

Corresponding author: Claudia.schroderadams@carleton.ca

Keywords: Cenomanian/Turonian Boundary Interval, High Arctic Large Igneous Province, $^{187}Os/^{188}Os$ isotope composition, Carbon isotopes, Arctic Sverdrup Basin, Foraminifera

Abstract

Emplacement of Large Igneous Provinces (LIPs) had a major effect on global climate, ocean chemistries as traced in sedimentary records and biotic turnovers. The linkage between LIPs and oceanic anoxic events has been documented with the Cenomanian/Turonian boundary event and Oceanic Anoxic Event 2 (OAE2). The Caribbean LIP and High Arctic Large Igneous Province (HALIP) are regarded as possible triggers. The pericratonic Arctic Sverdrup Basin is the partial location of the HALIP, where little is known about sedimentary, geochemical and biotic responses to the HALIP phases. Sedimentary strata at Glacier Fiord, Axel Heiberg Island, exhibit a dynamic Cretaceous polar carbon burial history within the lower to middle Cenomanian Bastion Ridge Formation and upper Cenomanian to Turonian part of the Kanguk Formation. We present the first initial $^{187}Os/^{188}Os$ (Os_i) composition profile for a polar Cenomanian/Turonian boundary interval (~100-93.9 Ma) linked to recently dated magmatic phases of the Strand Fiord Formation, part of the HALIP. The carbon isotope record coupled with the Os_i profile show two events in the upper Cenomanian interval marked by positive carbon perturbations and shifts to more non-radiogenic Os_i compositions. The earlier short-lived event is interpreted as result of weathering of the surrounding Strand Fiord volcanics causing a local non-radiogenic Os_i signal. Coinciding transgressive shorelines let to an increase in marine and terrestrially derived organic matter. Subsequently, injection of mantle-derived basalts into organic rich sediments is credited with causing the release of methane documented in a distinct negative carbon isotope excursion. We speculate that the methane release of the HALIP was an important contribution for rapid global warming caused by increasing atmospheric CO_2 levels associated with the OAE2 event likewise recognized in the Sverdrup Basin. As climate cooled in the middle and late Turonian, carbon burial decreased under increasingly oxygenated benthic conditions. Epifaunal

foraminiferal species, adapted to low oxygen conditions, persisted during the OAE2. Our Cenomanian to Turonian multiproxy record of the Sverdrup Basin distinguishes between local and global signals within a restricted High Arctic basin. Our results demonstrate the interplay between basin tectonism and sea-level change, increased weathering during transgressive phases, seafloor processes such as hydrothermal activity and methane release and biotic response to a complex paleoceanography. With future reliable dated frameworks this unique polar record will facilitate correlations to other polar basins and records of lower paleolatitudes.

1. Introduction

The influence of Large Igneous Provinces (LIPs) on paleoclimate, ocean chemistries and paleoecosystems has become increasingly apparent (e.g., Erba et al. 2015; Ernst and Youbi, 2017). The contribution of these large magmatic events to global greenhouse climate phases is demonstrated at the Cenomanian/Turonian boundary event and the global Oceanic Anoxic Event 2 (OAE2) where the Caribbean Large Igneous Province (CLIP) is considered as the main causative driver (Snow et al., 2005; Holmden et al., 2016; Scaife et al., 2017). Although the High Arctic LIP (HALIP) is largely understudied it is also considered to be a driving mechanism of OAE2 (Tegner et al., 2011; Zheng et al., 2013). More recently, a chronological linkage between the LIP emplacement and the global carbon burial event is demonstrated with osmium isotope records (Turgeon and Creaser, 2008; Du Vivier et al., 2014; 2015).

Documentation of OAE2 in the Sverdrup Basin, a pericratonic basin located in the High Arctic Canadian Archipelago, is relatively new (Pugh et al., 2014; Lenniger et al., 2014; Herrle et al., 2015). The feedback mechanism between LIP emplacement and the Arctic Cenomanian/Turonian boundary event as recorded in the Arctic has not been investigated. In this respect the Sverdrup Basin is a promising site since it partially records the HALIP, where several

phases of magmatic activity can be distinguished (Tegner et al., 2011; Estrada and Henjes-Kunst, 2013, 2016; Jowitt et al., 2014; Saumur et al., 2016).

Glacier Fiord on Axel Heiberg Island in the Canadian High Arctic (Figs. 1A, B) provides a unique site, where Cenomanian/Turonian strata are well exposed in outcrop with a documented OAE2 interval (Schröder-Adams et al., 2014; Herrle et al., 2015). Furthermore, this site is near (~50 km) to the Strand Fiord Formation containing flood basalts (Fig. 1B) that are part of the younger HALIP phases ranging from 105 to 92 Ma (Villeneuve and Williamson, 2006; Estrada et al., 2016). The Strand Fiord volcanics are extensively exposed in the southern region of Axel Heiberg Island (Fig. 1B). Thus, this location offers a favourable geological setting to investigate the direct influence of a magmatic event that is part of a major LIP on geochemical cycling and marine ecosystems. To link the eruption of the Strand Fiord volcanics to polar and global paleoceanographic and paleoecosystem changes we apply carbon isotopes coupled with the first osmium isotope record ($^{187}Os/^{188}Os$) from the Cretaceous Sverdrup Basin, and selected whole rock geochemistry and Rock Eval analysis. Benthic redox conditions are corroborated with benthic foraminiferal abundances and morphotype distribution and paleoenvironmental interpretations are aided by palynomorph occurrences. Integration of these data allow us to: a) explore Cenomanian to Turonian carbon burial histories and geochemical changes within a polar basin; b) document linkages to the HALIP and ultimately the rifting history of the Amerasia Basin; and c) distinguish local from global paleoenvironmental controls on the Sverdrup Basin.

2. Geological Setting

2.1. The Cenomanian/Turonian boundary interval in the Sverdrup Basin

The Cenomanian/Turonian boundary lies within the lower Kanguk Formation, a mudrock dominated transgressive unit spanning the upper Cenomanian to Campanian in the Sverdrup

Basin (Embry and Beauchamp, 2008). Currently, three localities are described from the Canadian High Arctic where the Cenomanian/Turonian boundary interval with a pronounced positive $\delta^{13}C_{org}$ signal is reported. At Hoodoo Dome on Ellef Ringnes Island (Fig. 1A), representing a central basin position, OAE2 occurs within a silty shale at the base of the Kanguk Formation immediately overlying the deltaic sandstones of the Hassel Formation (Fig. 2) (Pugh et al., 2014). At May Point (east central Axel Heiberg Island, Fig. 1B), positioned closer to the eastern margin of the Sverdrup Basin, the OAE2 interval is characterized by 'paper shale' at the base of the Kanguk Formation (Lenniger et al., 2014). At Glacier Fiord (southern Axel Heiberg Island, Fig. 1B) with a similar basin position to May Point, the OAE2 interval is documented in a 'paper shale' within the lower Kanguk Formation (Herrle et al., 2015). At Glacier Fiord the Kanguk Formation overlies the Bastion Ridge Formation (Figs. 2, 3A), that in turn overlies the Hassel Formation (MacRae, et al., 1996; Schröder-Adams et al., 2014). The silty shale unit of the Bastion Ridge Formation is interpreted to record deposition in a regionally restricted basin (MacRae, 1992). In vicinity to Strand Fiord (Fig. 2) the Bastion Ridge Formation lies between the Hassel Formation and the Strand Fiord volcanics or is interbedded with the volcanics (Ricketts et al., 1985; MacRae et al., 1996); at Glacier Fiord, where no volcanics were deposited, the Bastion Ridge Formation separates the Hassel from the Kanguk Formation (Fig. 3A) (Schröder-Adams et al., 2014).

Benthic foraminifera at Glacier Fiord have been used to pinpoint the Albian/Cenomanian and Cenomanian/Turonian boundaries (Schröder-Adams et al., 2014). Carbon isotope records have clearly identified the position of the OAE2 interval (Herrle et al., 2015). In addition, several CA-ID-TIMS weighted $^{206}Pb/^{238}U$ zircon dates of bentonites (Fig. 4) including one from the Bastion Ridge Formation and five from the Turonian part of the Kanguk Formation above OAE2

111 have been determined (Davis et al., 2016). The bentonite in the middle of the Bastion Ridge
112 Formation yielded a weighted $^{206}Pb/^{238}U$ zircon age of 98.3 ± 1.8 Ma, suggesting a maximum
113 age for the sampled horizon. The stratigraphically oldest bentonite of the Turonian bentonite
114 swarm within the Kanguk Formation yielded a weighted $^{206}Pb/^{238}U$ zircon age of 93.03 ± 0.21
115 Ma. Coupling this age with the top of the positive carbon isotope excursion closely placed to the
116 Cenomanian/Turonian boundary at 93.9 Ma a sedimentation rate of 19 m Ma^{-1} is calculated for
117 the lower Turonian (Davis, et al., 2016).

118 *2.2. The HALIP and Strand Fiord Formation*

119 Volcanic and intrusive rocks of the HALIP are exposed in the Arctic region with large
120 volumes being mapped within the Sverdrup Basin on Ellef and Amund Ringnes, Axel Heiberg
121 and Ellesmere islands (e.g. Embry and Osadetz, 1988; Ricketts et al., 1985; Estrada and Henjes-
122 Kunst, 2004, 2013; Buchan and Ernst, 2006; Evenchick et al., 2015). Two dominant pulses are
123 recognized, an older phase dominated by tholeiitic magmas spanning approximately 130 to ~83
124 Ma ago and a younger alkaline phase from 93 to 60 Ma (Embry and Osadetz, 1988; Tegner et al,
125 2011; Thorarinsson et al., 2011; Estrada et al., 2016). Of interest here is the last pulse of the
126 older phase associated with the volcanics of the Strand Fiord Formation.

127 The continental flood basalts of the Strand Fiord Formation (Souther, 1963;
128 Thorsteinsson, 1971; Ricketts et al., 1985) are exposed on the Kanguk Peninsula of Axel Heiberg
129 Island (Fig. 1B) where they reach a maximum thickness of ~950 m at Bunde Fiord (Williamson
130 et al., 2016), and thin towards the east and south (Ricketts et al, 1985; MacRae et al., 1996). At
131 Bunde Fiord subaerial lavas dominate, whereas at Strand Fiord lavas either overly or interfinger
132 with marine shales of the Bastion Ridge Formation. At Strand Fiord volcanic extrusion was
133 initially submarine and rapid build-up changed to a subaerial deposition. The Strand Fiord

Formation consists of tholeiitic icelandite flows (Pahoehoe and aa flows) with minor occurrences of epiclastic and pyroclastic components that increase towards the east and south with evidence of laharic flows reaching the marine basin. The thickness of individual flows ranges from 6 to 60 m (Ricketts et al., 1985). The Strand Fiord Formation is not present at the head of Glacier Fiord (Figs. 1B, 2).

Stratigraphically, the Strand Fiord volcanics overly the upper Albian to Cenomanian Hassel Formation (Figs. 2, 3B). No siliciclastic material of Hassel origin was found in the Strand Fiord volcanics (Ricketts et al., 1985). The volcanics overlie and partly interfinger with the time-equivalent Cenomanian Bastion Ridge Formation confirmed by injection structures at their contacts and the presence of bombs and lapilli-sized volcanic clasts within the upper Bastion Ridge Formation (Ricketts et al., 1985). The marine shales of the Kanguk Formation top the volcanics (Figs. 2, 3D; Ricketts et al., 1985; MacRae et al., 1996). Detailed mapping at Strand Fiord characterized two different eruption phases of the Strand Fiord volcanics (Ricketts et al., 1985; Williamson, 1988). Based on palynology of interlayered sedimentary strata a late Albian to early Cenomanian age was originally suggested for the Strand Fiord Formation (Ricketts et al., 1985; Embry and Osadetz, 1988; Nuñez- Betelu et al., 1994; MacRae et al., 1996) which represents an early precursor phase close to the Albian/Cenomanian boundary. A whole rock basalt $^{40}Ar/^{39}Ar$ age of 95.3 ± 0.2 Ma from the uppermost lava flow at Strand Fiord (Fig. 1B) constrains the later phase into the late Cenomanian (Tarduno et al., 1998). Furthermore, two separate feeder dykes related to the late Strand Fiord HALIP pulse close to South Fiord on Axel Heiberg Island (Fig. 1B) delivered U-Pb CA-ID-TIMS $^{206}Pb/^{238}U$ zircon weighted average ages of 95.18 ± 0.35 Ma and 95.41 ± 0.12 Ma (Kingsbury et al., 2018). The emplacement/eruption duration of the late phase is considered to be < 1 myr (Kingsbury et al., 2018). These late

157 Cenomanian ages correlate well with age estimates derived from foraminiferal biostratigraphy
158 and carbon isotope stratigraphy (Schröder-Adams et al., 2014; Herrle et al., 2015) and a
159 bentonite age of <98.3 ± 1.8 Ma (Davis et al., 2016) of the Bastion Ridge Formation at Glacier
160 Fiord.

161 *2.3. Cenomanian/Turonian lithology at Glacier Fiord*

162 The Glacier Fiord section (N 78^{o} 37.795', W 89^{o} 53.682', Fig. 1B) discussed here covers
163 112 m that forms the entire Bastion Ridge Formation and 133 m of the overlying lower Kanguk
164 Formation. The Bastion Ridge Formation overlies a thin paleosol at the top of the Hassel
165 Formation, which represents the widespread Albian/Cenomanian disconformity (Embry and
166 Dixon, 1990; Schröder-Adams et al., 2014). The 112 m thick Bastion Ridge Formation consists
167 of a 70 m thick dark grey to black to rusty oxidized silty shale (Fig. 3C), containing very fine-
168 grained sandstone beds and siderite concretions and a 15 cm thick bentonite at 50 m. This
169 interval is followed by a 10 m thick bioturbated sandstone that contains a lower 6 m thick yellow
170 to brown unit and a 4 m thick upper grey unit (Fig. 3C). This is followed by a 7 m thick covered
171 interval overlain by 25 m of silty mudrock with several distinct siderite beds (Fig. 4) interpreted
172 as freshwater siderites (Ross et al., in press), which suggests a possible hiatus in the middle
173 Cenomanian (Fig. 4). At 112 m the lithology changes abruptly to dark grey 'paper shale'
174 marking the base of the transgressive Kanguk Formation. The nearly 500 m thick formation
175 (Schröder-Adams et al., 2014) of which the lower 135 m are discussed here are interbedded with
176 frequent bentonites.

177 Geochemical and isotope data and details of section correlation, materials and analytical
178 methodologies are presented in the Supplementary Materials.

3. Results

3.1. Carbon and Osmium Isotope Stratigraphy

The existing $\delta^{13}C_{org}$ stratigraphy of the Glacier Fiord locality (Herrle et al., 2015) is further refined here with additional data points (Fig. 4, Table 2) from 85 m to 132 m to improve the resolution within the Cenomanian/Turonian boundary interval. The lower to middle Bastion Ridge Formation (0 to 72 m, Fig. 4) is characterized by only small variation (-25.7 to 24.8 ‰) in $\delta^{13}C_{org}$ with increasingly positive values towards the top at 70 m. The TOC values vary between 0.7 to 4.5 %. $\delta^{13}C_{org}$ values in the uppermost Bastion Ridge interval show a slight switch of 1‰ to more negative values at about 95 m, corresponding to low TOC values of close to 1 %. The uppermost 7 m of the Bastion Ridge Formation (105 to 112 m) show an increase of ~0.5 ‰ to more positive values (Fig. 4). Just above the basal boundary of the Kanguk Formation at 112 m a significant, short-lived positive $\delta^{13}C_{org}$ excursion of 2 ‰ is coupled with the onset of organic-rich platy shale and significant, but brief increase in TOC (10.9 %). Initially, this sustained increase in TOC content corresponds to a strong negative excursion of 1.5 ‰ in the interval between 122 to 130 m. The most significant positive $\delta^{13}C_{org}$ excursion of >2 ‰ representing OAE2 occurs in the lower Kanguk Formation between 131 to 152 m and is accompanied with elevated, but fluctuating TOC values of up to 10 %. Above 152 m $\delta^{13}C_{org}$ values stay initially light and become gradually heavier throughout the middle to upper Turonian interval.

The Re abundance of the Bastion Ridge Formation shows little variation (0.2 to 1.2 ppb; Fig. 4; Table 3). Noticeable enrichments in Re abundance are shown by a minor peak at 112 m of 5.2 ppb at the base of the Kanguk Formation, and in the ~127 m interval where Re increases to 13.3 ppb and then decreases to ~1-3 ppb. The ^{192}Os abundance profile (the best estimate of Os chelated at the time of deposition) shows a similar trend to that of Re. In that, the ^{192}Os

abundance is relatively uniform within the Bastion Ridge Formation (5 to 40 ppt; Fig. 4; Table 3). As shown for Re in the ~127 m interval, a significant increase in ^{192}Os (up to 388 ppt) is observed. However, no ^{192}Os enrichment is observed at the 112 m level where an enrichment in Re of 5.2 ppb is shown.

In contrast to the Re and Os abundances, the initial $^{187}Os/^{188}Os$ (Os_i) compositions through the Bastion Ridge and Kanguk formations are distinctly different. The Os_i values are calculated at 94 Ma. As discussed above and below, part of the Bastion Ridge Formation is appreciably older (~98 Ma) however, given the overall low Re abundance of the samples from the Bastion Ridge Formation, the additional age correction equates to a difference smaller than the uncertainty in the Os_i value (Table 3). As such, the Os_i profile shown in Figure 4 remains essentially the same.

In the Bastion Ridge Formation between 5 and 25 m the Os_i compositions are relatively uniform at ~0.55 (Fig. 4). From ~25 to 65 m the Os_i values become increasing more radiogenic reaching a maximum of ~0.7. The Os_i values become less radiogenic over the following ~10 m, to just beneath the freshwater siderite (Ross et al., 2018).

From the intervals at 87 to 105 m in the upper Bastion Ridge Formation the Os_i values become increasingly more radiogenic (~0.4 to 0.6), and then become slightly more less radiogenic to 111 m where the Os_i values show an abrupt shift to ~0.2 and return to ~0.4, where the Os_i then exhibit a very nonradiogenic shift to ~0.1 at 114 m in the basal Kanguk Formation. From 114 m the Os_i values abruptly return to radiogenic value of 0.70 for 10 m, and then at 125 m become nonradiogenic within the negative pronounced trend of the $\delta^{13}C$ profile and below the abrupt positive $\delta^{13}C$ excursion interpreted that marks the onset of the OAE2 interval.

Nonradiogenic Os_i compositions (Os_i = ~0.2) continue for ~20 m before returning to more radiogenic compositions of ~0.7 (Fig. 4; Table 3).

3.2. Geochemical cycling

Here we apply, Zn/Al and Mn/Al and Fe records to investigate magmatic/hydrothermal contributions (Liao et al., 2018) to the Bastion Ridge and Kanguk formations (Fig. 4). The Zn/Al distribution is variable throughout the section with consistently highest values in the uppermost silty mudrock interval of the Bastion Ridge Formation (up to 100) and one peak (82) in the upper interval of OAE2 (141 m) and a minor increase (17) at about 180 m within an interval marked by numerous interbedded bentonite horizons. The Mn/Al values show two peaks at the base of and in the uppermost Bastion Ridge Formation, correlating with the increased Zn/Al record. The Zn/Al and Mn/Al records both show a significant increase at the base of the negative $\delta^{13}C$ excursion. The Fe abundance peaks at the base of the Bastion Ridge Formation (1 and 5 m) and is elevated between 50 - 70 m (Fig. 4). Ratios of TOC (%) / Sulfur content (%) are plotted to distinguish between marine and freshwater or slightly brackish regimes (Berner and Raiswell, 1984). A higher ratio within the Bastion Ridge Formation confirms its brackish to freshwater nature compared to the marine Kanguk Formation. The lowermost two samples in the Bastion Ridge Formation form the exception indicating short-lived marine influence (Fig. 5).

3.3. Foraminifera, palynomorph and paleoproductivity records

The presence/absence of benthic foraminifera and their morphotype distribution permits evaluation of benthic redox conditions (Nagy, 1992; Jorissen et al., 1995; Herrle et al., 2003; Murray et al., 2011; Quesnel et al., 2017), which can then be compared with the carbon burial history (Fig. 6). Only benthic foraminifera were recovered from the sample set and are absent in

intervals dominated by terrestrial and freshwater conditions such as most of the Bastion Ridge Formation (4 to 112 m). Two additional barren intervals are notable; these are within the interval of the lower positive carbon isotope excursion at ~112 m and right after OAE2 at 145 – 155 m, but not within the OAE2 interval (Fig. 6).

Three morphotypes were distinguished (Fig. 6) including: a) infaunal deposit feeders with elongated, multichambered tests, preferring mesotrophic to eutrophic environments that are often oxygen-poor; b) shallow infaunal to epifaunal deposit feeders with coiled tests, adapted to oxygenated, oligotrophic conditions; and c) epifaunal assemblages dominated by the genus *Trochammina*, tolerant to reduced benthic oxygen conditions under high organic matter supply (Gooday et al., 2000). The limited presence of benthic foraminifera at the base of the Bastion Ridge Formation indicates a short marine phase which confirms the low marine TOC/S ratios in those samples (Figs. 5, 6). The 'paper shale' unit of the basal Kanguk Formation including the OAE2 interval is dominated by epifaunal taxa with minute tests, mainly of the genus *Trochammina*. This genus has previously been related to depleted oxygen conditions of the Toarcian Oceanic Anoxic Event (Reolid et al., 2014). Toward the top of OAE2 the highest concentration of Mo (up to 8 ppm) occurs, a redox-sensitive trace metal that is enhanced under sulfidic conditions (Helz et al., 1996). This interval (145 to 150 m) coincides with a reduction in benthic fauna that does not recover for some time after OAE2 (Fig. 6). Finally, the upper Turonian interval is characterized by increasingly diverse assemblages with all three morphotypes represented (Fig. 6).

The uppermost Bastion Ridge Formation is dominated by the non-marine dinocysts *Nyktericysta* sp. and *Vesperopsis* sp. of freshwater and brackish origin (Mao et al., 1999). The non-marine acritarch *Limbicysta* sp. (MacRae et al. 1996) also has a common occurrence within

this interval; thereby, clearly confirming the placement of a terrestrially influenced unit in the uppermost Bastion Ridge Formation. As the lithology changes to 'paper shale' in the basal Kanguk Formation non-marine dinocysts and acritarchs disappear. Marine dinocysts appear in small numbers with abundant amorphous organic matter. Pollen are abundant, and the interval marked by the first pronounced negative $\delta^{13}C_{org}$ excursion is particularly dominated by wind-blown bisaccates (Mudie, 1982). Within the actual OAE2 interval bisaccates lose their dominance.

Hydrogen Indices (HI) vary around 50 $mgCO_2/gOC$ in the Bastion Ridge Formation supporting a terrestrial source. Within the Kanguk Formation HI values increase, ranging from 300 and 400 $mgCO_2/gOC$ and coinciding with peaks in TOC at 114 m and within OAE2 suggesting an increasing marine organic matter source. At 170 m HI values return to terrestrial signals (Fig. 6).

4. Age Model of the Cenomanian/Turonian interval at Glacier Fiord

The stratigraphic age model for the Glacier Fiord section is based on extrapolation using proposed sedimentation rates where from 167 to 203 m five bentonite beds yield weighted $^{206}Pb/^{238}U$ zircon CA-ID-TIMS dates of 93.03 ± 0.21 to 91.02 ± 0.3 Ma (Fig. 4; Davis et al., 2016). A sedimentation rate of 19 m Ma^{-1} is calculated (Davis, et al., 2016) for the strata between the oldest dated bentonite (93.03 ± 0.21 Ma) and the established age of the Cenomanian/Turonian boundary (93.9 Ma) (Gradstein et al., 2012; Meyers et al., 2012; Du Vivier et al., 2015) as placed close to the top of the OAE2 interval at 151 m. Lithologies in the lower Kanguk interval are relatively even dominated by 'paper shale' with the occasional silty interbeds suggesting a similar sedimentation rate of 19 m Ma^{-1} throughout. It is noted, however,

that some uncertainty could be caused by the position of the lowest dated bentonite within two covered intervals where exact measurement of the section thickness might be slightly obscured.

Using the sedimentation rate of 19 m Ma^{-1} an approximate age of six intervals associated with significant changes in the $\delta^{13}C_{org}$ and Os_i records are calculated (Fig. 4). These include in ascending stratigraphic order: 1) the base of the Kanguk Formation at 112 m and onset of 'paper shale' at ~95.92 Ma (level F); 2) the horizon at 114 m with the peak in TOC, $\delta^{13}C_{org}$ and non-radiogenic Os_i pulse at ~95.81 Ma (level E); 3) the horizon at 125 m reflecting the first non-radiogenic Os_i value from the prolonged non-radiogenic signal at ~95.24 Ma (level D); 4) the base of the positive $\delta^{13}C$ excursion at 131 m interpreted as OAE2 at ~94.92 Ma (level A); 5) the interval of the first slight negative shift in $\delta^{13}C$ at 137 m within OAE2 at ~94.6 Ma (level B); and 6) the top of OAE2 at 151 m where the $\delta^{13}C$ values return to more negative at ~93.87 Ma (level C).

Globally the positive $\delta^{13}C$ values of OAE2 is described with three datum levels (maintained here), where A marks the base of the positive excursion, B a trough after the first positive excursion and C the level of the last positive $\delta^{13}C$ value (Pratt et al., 1985; Tsikos et al., 2004; Forster et al., 2007). Using the latest $^{206}Pb/^{238}U$ zircon CA-ID-TIMS calibrated ages (Du Vivier et al., 2015), the first least nonradiogenic Os_i value dated at ~94.44 ± 0.14 Ma falls stratigraphically below Datum A and being hence a few tens of thousands of years younger. This agrees with the interpolated age from the Western Interior Seaway (WIS) OAE2 section (Meyers et al., 2012; Du Vivier et al., 2015; Kuhnt et al., 2017). These dates coupled with the timing of Datum C (93.92 Ma) yield an OAE2 duration of approximately 600 kyr years (Meyers et al., 2012; Du Vivier et al., 2015). In contrast, notwithstanding argument of inheritance within the CA-ID-TIMS zircon ages, constraints of the OAE2 interval of the Iona-1 core of western Texas,

USA extended the duration of OAE2 to approximately 900 kyr moving the base down to include what Eldrett et al. (2014) called the precursor events of OAE2 (Jenkyns et al., 2017).

The importance of these calculated dates at the Glacier Fiord section results in the exclusion of the positive excursion in $\delta^{13}C_{org}$ at 114 m from the OAE2 interval (Fig. 4). This isotopically heavy carbon value at 114 m, although represented only by one measurement, is significant given that a time equivalent environmental perturbation is also recognized by a significant increase in TOC (~11 %), a clear shift to non-radiogenic Os_i and an increase in Re abundance (Fig. 4). As the shale lithology persists down to 112 m in the section we use the same sedimentation rate of 19 m Ma^{-1}, to place the $\delta^{13}C_{org}$ excursion at ~95.81 Ma (Level E).

Further, proposing an absolute age framework for the Bastion Ridge Formation becomes more difficult due to the disconformities of unknown duration that would be associated with the uppermost Bastion Ridge Formation (86 to 110 m) and markedly changing lithologies within the formation. The proposed age of approximately 96 Ma for the base of the Bastion Ridge Formation (Herrle et al., 2015) requires revision. A bentonite at 50 m within the middle of the Bastion Ridge Formation yields a weighted average $^{206}Pb/^{238}U$ zircon CA-ID-TIMS minimum age of <98.3 ± 1.8 Ma (Davis et al., 2016) suggesting that the basal boundary could be closer to the Albian/Cenomanian boundary (100.5 Ma; Gradstein et al., 2012) and the hiatus might be of small duration.

Based on the youngest dated bentonite unit, the upper part of the Glacier Fiord section studied here is younger than 91.02 ± 0.3 Ma (Davis et al., 2016). Biostratigraphic markers of *Scaphites corvensis* and *S. nigricollensis* at 240 m in the upper Glacier Fiord section suggests a latest Turonian age (~90.5 Ma; Schröder-Adams et al., 2014).

5. Discussion

The Cenomanian/Turonian boundary interval at Glacier Fiord offers a locality in close vicinity to contemporaneous magmatic activities of the younger HALIP phases. In localities north of Glacier Fiord, where the Strand Fiord volcanics are mapped (Fig. 1), the Bastion Ridge Formation occurs either below the volcanics or interfingers with the volcanics (Fig. 3; Ricketts et al., 1985; MacRae et al., 1996; Williamson, 2016). The Kanguk Formation conformably to unconformably overlies the Strand Fiord Formation. Thus, the likelihood of direct magmatic control on ocean geochemistry and local ecosystems is high. The interaction between basin events, geochemical cycling and biotic response is discussed for five distinct stages that mark the Cenomanian to Turonian interval in this polar locality.

5.1. Bastion Ridge Formation – tectonic setting and paleoenvironment

Stratigraphically, the regionally restricted Bastion Ridge Formation is time equivalent with the upper Hassel Formation elsewhere (Fig. 2). Our reconstructions at Glacier Fiord place a Cenomanian age on the Bastion Ridge Formation. On Ellef Ringnes Island (Fig. 1A), the Hassel Formation ranges up into the Cenomanian (Galloway et al., 2012; Pugh et al., 2014), and it is the Cenomanian part that is equivalent to the Bastion Ridge Formation (Fig. 2). Whereas the surrounding Hassel Formation represents extensive shoreface, and deltaic deposits, the tectonic and depositional paleoenvironment of the Bastion Ridge Formation is interpreted as a restricted basin possibly related to a graben structure resulting in a protected embayment as the result of tectonic basin extension (Embry and Osadetz, 1987; MacRae, 1992). This restricted basin was marine in its initial phase supporting a foraminiferal assemblage (Fig. 6; Schröder-Adams et al., 2014), but became more brackish and terrestrial up section (Fig. 5) with increasing amounts of brackish acritarchs and terrestrial pollen, respectively (MacRae et al., 1996). This interpretation

359 is supported by the Os_i values, whereby the Os_i values become increasingly more radiogenic
360 from a background value of ~0.5 to 0.8. The increasingly terrestrial nature of the Bastion Ridge
361 Formation is explained by uplift and possibly doming associated with the coeval eruption of the
362 Strand Fiord basalts (Dostal and MacRae, 2017) resulting in basin restriction. Phases of Mn, Zn
363 and Fe enrichment (Fig. 4) at the base of the Bastion Ridge Formation might be explained by
364 hydrothermal activity in the marine phase of the rift basin (German and Von Damm, 2006).
365 Later, geochemical signatures were also influenced by weathering of the surrounding Strand
366 Fiord volcanics as their eruptions might have further restricted the basin from marine influence.
367 Low TOC content and HI values (Fig. 6) point towards low to non-existing marine productivity
368 confirming faunal interpretations and low terrestrial organic matter input due to surrounding
369 volcanics without vegetation. The $\delta^{13}C_{org}$ record lacks any perturbations in a time where only
370 one preserved bentonite attests to a relatively quiet phase of volcanism throughout the early
371 Cenomanian. The overlying sandstone between 70 and 80 m is interpreted as a shoreface
372 sandstone, where bioturbation suggests a brief return to marine influence. This influence is
373 recorded in the Os_i values, where they become slightly less radiogenic. Within the middle
374 Cenomanian uppermost Bastion Ridge Formation freshwater siderite beds developed (Ross et al.,
375 in press). The presence of acritarchs gives evidence for intermittent brackish water influence and
376 coincide with more radiogenic Os_i values (~0.5 to 0.7).

377 Of interest in this interval is the $\delta^{13}C_{org}$ record which initially shows a couple of negative
378 excursions followed by a minor short-lived positive one between 108 and 110 m. Since the
379 overlying boundary between the Bastion Ridge/Kanguk formations is dated at ~95.92 Ma this
380 switch to positive $\delta^{13}C_{org}$ values falls closely to the age of the Mid-Cenomanian Event (MCE)
381 with an age of ~96 Ma (Paul et al. 1994; Jarvis et al., 2006; Joo and Sageman, 2014; Zhang et al.,

2016). The position of this interval in the uppermost terrestrial Bastion Ridge Formation (Fig. 6) might explain the weak positive $\delta^{13}C$ expression caused by terrestrial influence. Thus, correlation to marine MCE records elsewhere remains tentative. This event is immediately followed by a minor shift towards non-radiogenic Os_i values marked by level F and dated at 95.92 Ma (Fig. 4).

5.2. Kanguk Formation – the early transgressive phase

Embry and Osadetz (1988) assigned an approximate age of 95 Ma to the transition of the main rifting phase of the Canada Basin to a time of seafloor spreading, which consequently lasted for the next 25 myr (Fig. 2). At Glacier Fiord the upper Middle Cenomanian lithological change to marine 'paper shale' at 112 m in the section (Figs. 2, 3A, 4, 6) marks a phase of major basin subsidence and rapid transgression transforming this site into a shelf environment largely below storm wave base. Basin wide, the basal boundary of the Kanguk Formation is diachronous by using the position of the OAE2 positive carbon excursion as a chronostratigraphic marker (Davies et al., 2018). At Glacier Fiord the base of the Kanguk Formation falls at ~ 95.92 Ma. The depositional change is followed by a short lived positive $\delta^{13}C_{org}$ perturbation (level E at ~95.81 Ma, Fig. 4). Organic matter of dominantly terrestrial origin (Type III) swept into the basin through a transgressive shoreline (Fig. 6). A phase of increased paleoproductivity including marine dinoflagellates, stimulated by increased nutrient supply, and terrestrial organic matter input extended the oxygen minimum zone, which resulted into absence of benthic foraminifera. Relative abundance of wind-blown bisaccates decrease in abundance and terrestrially derived pollen increase. At the same time, a single sample shows a significant change to non-radiogenic Os_i values, a minor peak in Re abundance, but no change in ^{192}Os abundance. This is interpreted as the result of flooding the extensive Strand Fiord volcanics as a source of non-radiogenic Os. The organic-rich nature of this interval may explain the peak in Re as it acted as a sink for

dissolved Re in seawater (Jaffe et al., 2002). The return to radiogenic Os_i at 116 m correlates to an interval dominated by siltstone beds pointing towards increased crustal weathering and greater shoreline proximity.

5.3. A negative carbon isotope excursion - a precursor to the Arctic OAE2 interval

Level D (Fig. 4) dated at ~95.24 Ma is marked by the return to non-radiogenic Os_i, a peak in ^{192}Os and Re abundance. This age closely correlates to the $^{40}Ar/^{39}Ar$ age of 95.3 ± 0.2 Ma from the uppermost lava flow at Strand Fiord (Tarduno et al., 1998) and the age of 95.18 ± 0.35 Ma and 95.41 ± 0.12 Ma of two separate feeder dykes related to the late Strand Fiord HALIP pulse (Kingsbury et al., 2018) suggesting a possible link and local influence (Fig. 4). The non-radiogenic Os_i excursion at ~125 m places stratigraphically below the well-documented global signature of non-radiogenic Os_i at the base of OAE2 with a younger age of ~94.4 Ma, which is followed by a gradual return to radiogenic values (Du Vivier et al., 2014, 2015). The earlier signal might be explained by local basin processes and/or age uncertainties of the Arctic site.

Level D is within a distinct negative $\delta^{13}C_{org}$ excursion that precedes the OAE2 positive excursion. The upper shift to non-radiogenic Os_i values between 120 to 125 m corresponds directly with the base of the negative $\delta^{13}C_{org}$ trend. The timing of this shift roughly corresponds to established ages of the late Strand Fiord HALIP pulse (Kingsbury et al., 2018). Two scenarios might explain the shift to non-radiogenic Os_i. If magmatism was submarine at this time hydrothermal fluids were injected into the ocean. If the HALIP pulse was dominantly subaerial, the Os record provides a weathering signal. The most negative $\delta^{13}C_{org}$ interval at Glacier Fiord corresponds with the appearance of the first of several bentonites that become more common during OAE2 alluding to nearby volcanism of possible HALIP origin. One explanation for this shift to negative values might entail methane release due to mantle-derived intrusions into

organic-rich sediments of the Kanguk Formation (Fig. 4). Rapid heating of organic matter through intrusive activity might have caused contact metamorphism and triggered sharp negative carbon excursions caused by release of ^{13}C depleted carbon gases such as methane. A similar mechanism is reported from the Toarcian Oceanic Anoxic Event and Early Eocene climate maximum (Svensen et al., 2004, 2009; Aarnes et al., 2011). Detailed correlations between these processes in the Sverdrup Basin require additional data and a more refined timeframe.

The distinct negative $\delta^{13}C$ excursion below OAE2 as seen at Glacier Fiord at ~95 Ma appears to be only broadly contemporaneous with a distinct negative $\delta^{13}C$ excursion that straddles the Middle to Late Cenomanian Boundary in the Natih Formation, Oman, which consists of interbedded argillaceous and carbonate sediments (Wohlwend et al., 2016). Local diagenetic processes within an intra-platform basin including sulphate reduction and anaerobic oxidation of methane are invoked to cause the carbonates to be depleted in ^{13}C. As such additional Arctic records are needed to pinpoint the cause and possible connection with the HALIP phase.

5.4. The polar OAE2 interval

The positive $\delta^{13}C_{org}$ excursion denoting OAE2 is clearly expressed in the Glacier Fiord section and is marked with the traditionally used levels of A, B and C (Fig. 4). As magmatic activity and methane release ceased the carbon isotope signal resembles the global one. Its earlier diachronous base compared to the Yezo Group of Japan, the Greenhorn Formation of the Western Interior of the USA, and the OAE2 section in core SN˚4 of the Tafaya Basin, Morocco (Fig. 4, Du Vivier et al., 2015; Kuhnt et al., 2017) might be the result of some local influence on the $\delta^{13}C_{org}$ record. Influences in restricted basins might include surface water productivity, input

of organic matter from land, remineralization in the water column, carbonate and organic composition of the sediments and sea-level changes (Wagner et al., 2018 and references therein). The change to more positive $\delta^{13}C_{org}$ values is rapid and the lithology does not show any evidence for a disconformity. The age of Level B denotes a trough in the positive $\delta^{13}C_{org}$ excursion and falls at ~94.6 Ma. At this interval the Os_i gradually return to radiogenic signatures. Further, benthic foraminifera increase in diversity and abundance at this level which suggests an increasingly oxygenated basin. This coincides with a drop in TOC and HI values (Fig. 6). Although we have no Cenomanian/Turonian aged paleotemperature data from the Sverdrup Basin, combined evidence shows that the Plenus Cold Event can be detected. Paleotemperature proxies (TEX_{86}) have established a cooling trend at level B within the equatorial Atlantic (Sinninghe Damsté et al., 2010; van Helmond et al., 2013).

Level C marks the top of OAE2 and an abrupt return to lighter carbon isotopes. Although this abrupt change could suggest the presence of a hiatus, no lithological evidence for erosion was discovered. Above this level TOC content and HI values remain relatively high for another 10 m within the lower Turonian. A comparable relatively abrupt change to increasingly more negative $\delta^{13}C_{org}$ values was described from the Demarara Rise of the western equatorial Atlantic (Forster et al., 2007) where interval C marks the recovery phase above the C/T boundary. Their equatorial paleotemperature values denote a continued high sea surface temperature for the lower Turonian. At Glacier Fiord moderate HI values reaching up to 350 $mgCO_2/gOC$, abundant amorphous organic matter and a relatively poor, but diverse, marine dinoflagellate assemblage suggests a sustained input of terrestrial material into the basin throughout OAE2 that was supported by a climate regime of a warm and vegetated Arctic. At the Cenomanian/Turonian boundary interval at May Point (Axel Heiberg Island, Fig. 1B), a persistently anoxic water

column was interpreted based on Fe_{Hr}/Fe_T data (Lenniger et al., 2014). At Glacier Fiord, benthic foraminiferal assemblages are characterized by reduced species richness and in some samples a dominance of epifaunal minute *Trochammina* specimens indicating stressed benthic paleoenvironments in suboxic conditions. Varying TOC values throughout the OAE2 interval might indicate a combination of varying supply of organic matter including marine productivity and shifting redox conditions.

5.5. Middle to Late Turonian – cooling and benthic recovery

In the middle to upper Turonian interval lithologies have an increased abundance of silt and are interbedded with frequent bentonite beds resulting partially from the Wootton Intrusive Complex on Ellesmere Island (92.7 ± 0.3 Ma to 92 ± 0.1 Ma, Estrada and Henjes-Kunst, 2013) or from another volcanic phase in the Amerasia Basin (Davis et al., 2016). The $\delta^{13}C_{org}$ gradually increase towards more positive values and low TOC values suggest a more oxygenated ocean under globally cooler conditions (Friedrich et al., 2012). Benthic foraminiferal assemblages become more diverse with different morphotypes (Fig. 6). HI values give no indication for marine primary productivity possibly inhibited by increasingly abundant detrital material in surface waters. The peak in zinc enrichment between 180 and 200 m (Fig. 4) that coincides with the interval of frequent bentonite occurrences might be the result of the capacity of bentonites to absorb zinc (Sheta et al., 2003).

6. Conclusions

The Arctic Sverdrup Basin is the partial locale of the HALIP, a magmatic event that was suggested besides the Caribbean LIP as a controlling force for the oceanic osmium isotope stratigraphic profile within the Cenomanian/Turonian boundary interval. Correlations between

Os_i and $\delta^{13}C_{org}$ records mark a rapid shift to non-radiogenic Os_i values at the base of the OAE2 interval in open ocean settings suggesting LIP emplacement as one of the trigger mechanisms for OAEs. Smaller basins show the accentuation of precursor signals that might refer to local processes. This study makes the first direct comparison between ocean geochemical profiles and HALIP phases for an Arctic Cenomanian/Turonian boundary interval and reveals the sensitivity of ocean chemistry within a complex basin setting.

1. The dominantly brackish to terrestrial Bastion Ridge and marine Kanguk formations at Glacier Fiord provide a polar paleoenvironmental response to the globally recognized Cenomanian to Turonian carbon perturbations in close vicinity to one of the major LIP events, namely the Strand Fiord phase of the HALIP. The sequence of two events, as clearly displayed in carbon and osmium isotopic records, makes an argument for the control of local magmatic events on chemical cycling and ecosystem response within this High Arctic Cenomanian/Turonian boundary interval.

2. The basal interval of the Kanguk Formation records two phases of non-radiogenic osmium input; the first at ~95.8 Ma was short lived interpreted as a product of weathering of the Strand Fiord volcanics, that formed a topographic high at the time of Kanguk transgression. The second phase at ~95.2 Ma with a gradual return to radiogenic Os_i values represents the open ocean signal of a LIP and coincided with a major pulse of the Strand Fiord volcanics that were extruded near to the Glacier Fiord locality. Additional data are required to calibrate the Arctic record partially driven by local processes, with the global, open ocean record.

3. As in other restricted basins the polar Sverdrup Basin accentuated a local signal of a distinct negative carbon isotope excursion that predated the global signal of the OAE2 which might have

been the result of coeval intrusion of mantle-derived material into organic-rich shale causing carbon dioxide and methane release.

4. Ultimately global climate warmed and increasing amounts of marine and terrestrially derived organic matter was buried in the Sverdrup Basin resulting in a distinct positive carbon isotope excursion identified as OAE2 in the Arctic with a minimum duration of ~0.5 myr.

5. Benthic foraminifera and their morphogroup distributions allude to a basin of variable benthic redox conditions throughout its fully marine phases. Whereas anoxic phases barren of foraminifera existed, these did not occur during the OAE2 interval. There, assemblages of epifaunal species, tolerant to relatively low bottom water oxygen conditions, persisted giving testimony to suboxic conditions that still supported life.

The Glacier Fiord record is the first attempt to link carbon and osmium isotope records to the HALIP phase and consequently has constrained the Late Cretaceous Arctic stratigraphic framework. Our data has shed light on the complex interplay between subaerial versus submarine magmatic events, their linkage to regressive/transgressive phases; paleoceanographic responses to methane release and hydrothermal activity and ecosystem response. Our interpretations require future testing in the Sverdrup, Amerasia and Eurasia basins to evaluate further the influence of HALIP phases on paleoceanographic events. Future correlations require reliable age frameworks which then will allow increasingly global correlations and the identification of dominant large-scale earth processes.

Acknowledgement

We are grateful to the Nunavut Research Institute, Nunavut Water Board and Nunavut Department of Culture and Heritage for granting us the scientific research licenses. We like to thank the community of Grise Fiord for their agreement to conduct research on northern lands. Keenan Lindell is thanked for valuable field support and Craig Day for discussions on geochemical data. Denise Then, Mark Bujaki and Global Geolab LTD are thanked for sample preparation. Ross Stewart and Krista Boyce are thanked for Rock-Eval analysis. We thank Jens Fiebig and Bärbel Schminke for stable isotope and TOC measurements. Alice Du-Vivier, Chris Ottley, Geoff Nowell and Antonia Hofmann are thanked for laboratory support. We express our sincerest gratitude to the reliable staff and pilots of the Polar Continental Shelf Program who provided unfailing logistical support in the North. Two anonymous reviewers provided constructive comments that improved the manuscript. Financial support to Schröder-Adams was provided by a CRD Grant of the Natural Sciences and Engineering Research Council (NSERC) with the Geo-mapping for Energy and Minerals (GEM) Program of the Geological Survey of Canada and ConocoPhillips Houston and Calgary as partners. Financial support to Herrle was provided by the German Research Foundation (DFG) (HE 3521/6). DS acknowledges the Total Endowment Fund and the CUG Wuhan Dida Scholarship.

References

Aarnes, I., Svensen, H., Polteau, S., Planke, S., 2011. Contact metamorphic devolatilization of shales in the Karoo Basin, South Africa, and the effects of multiple sill intrusions. Chemical Geology, 281, 181-194.

Berner, R.A., Raiswell, R., 1984. C/S method for distinguishing freshwater from marine sedimentary rocks. Geology, 12, 365-368.

561 Buchan, K.L., Ernst, R., 2006. Giant dyke swarms and the reconstruction of the Canadian Arctic
562 islands, Greenland, Svalbard and Franz Josef Land. In Hanski, E., Mertanen, S., Rämö, T.,
563 Vuollo, J. (eds.). Dyke swarms – Time markers of crustal evolution, Taylor & Francis,
564 London, p. 27-48.
565 Davies, M.A., Schröder-Adams, C.J., Herrle, J.O., Hülse, P., Schneider, S., Quesnel, A.,
566 Harwood, D., 2018. Integrated bio- and carbon isotope-stratigraphy for the Upper Cretaceous
567 Kanguk Formation of the High Arctic Sverdrup Basin, Canada. Geological Society of
568 America, Bulletin, DOI: 10 .1130 /B31858 .1.
569 Davis, W.J., Schröder-Adams, C.J., Galloway, J.M., Herrle, J.O., Pugh, A.T., 2016. U-Pb
570 geochronology of bentonites from the upper Cretaceous Kanguk Formation, Sverdrup Basin,
571 Arctic Canada: constraints on sedimentation rates, biostratigraphic correlations and the late
572 magmatic history of the High Arctic Large Igneous Province. Geological Magazine, DOI:
573 10.1017/S0016756816000376.
574 Dostal, J., MacRae, A., 2017. Cretaceous basalts of the High Arctic Large Igneous Province at
575 Axel Heiberg Island (Canada): Volcanic stratigraphy, geodynamic setting and origin.
576 Geological Journal, DOI:10.1002/gj.3132.
577 Du Vivier, A.D.C., Selby, D., Condon, D.J., Takashima, R., Nishi, H., 2015. Pacific $^{187}Os/^{188}Os$
578 isotope chemistry and U-Pb geochronology: Synchroneity of global Os isotope change across
579 OAE 2. Earth and Planetary Science Letters, 428, 204-216.
580 Du Vivier, A.D.C., Selby, D., Sageman, B.B., Jarvis, I., Gröcke, D.R., Voigt, S., 2014. Marine
581 $^{187}Os/^{188}Os$ isotope stratigraphy reveals the interaction of volcanism and ocean circulation
582 during Oceanic Anoxic Event 2. Earth and Planetary Science Letters, 389, 23-33.

583 Eldrett, J.S., Minisini, D., Bergman, S.C., 2014. Decoupling of the carbon cycle during Ocean
584 Anoxic Event 2. Geology, 42 (7), 567-570.
585 Embry, A., Beauchamp, B., 2008. Sverdrup Basin, In Miall, A. (ed.). Sedimentary Basins of the
586 World, Volume 5, The Sedimentary Basins of the United States and Canada: Amsterdam,
587 Elsevier, p. 451–472.
588 Embry, A.F., Dixon, J., 1990. The breakup unconformity of the Amerasia Basin, Arctic
589 Ocean: Evidence from Arctic Canada. Geological Society of America Bulletin 102,
590 1526–1534.
591 Embry, A.F., Osadetz, K.G., 1988. Stratigraphic and tectonic significance of Cretaceous
592 volcanism in the Queen Elizabeth Islands, Canadian Arctic Archipelago. Canadian Journal
593 Earth Sciences, 25, 1209-1219.
594 Erba, E., Duncan, R.A., Bottini, C., Tiraboschi, D., Weissert, H., Jenkyns, H.C., and Malinverno,
595 A., 2015. Environmental consequences of Ontong Java Plateau and Kerguelen Plateau
596 volcanism. In Neal, C.R., Sager, W.W, Sano, T., and Erba, E. (eds.), The Origin, Evolution,
597 and Environmental Impact of Oceanic Large Igneous Provinces. Geological Society of
598 America Special Paper 511, 271–303, doi:10.1130/2015.2511(15).
599 Ernst, R.E., Youbi, N., 2017. How Large Igneous Provinces affect global climate, sometimes
600 cause mass extinctions, and represent natural markers in the geologic record.
601 Palaeogeography Palaeoclimatology Palaeoecology, DOI:10.1016/j.palaeo.2017.03.014.
602 Estrada, S., Damaske, D., Henjes-Kunst, F., Schreckenberger, B., Oakey, G.N., Piepjohn, K.,
603 Eckelmann, K., Linnemann, U., 2016. Multistage Cretaceous magmatism in the northern
604 coastal region of Ellesmere Island and its relation to the formation of Alpha Ridge-evidence

605 from aeromagmatic, geochemical and geochronological data. Norwegian Journal of Geology,
606 96 (2), 65-95.
607 Estrada, S., Henjes-Kunst, F., 2004. Volcanism in the Canadian High Arctic related to the
608 opening of the Arctic Ocean, Zeitschrift Deutsche Geologische Gesellschaft, 154, 579-603.
609 Estrada, S., Henjes-Kunst, F., 2013. ^{40}Ar-^{39}Ar and U-Pb dating of the Cretaceous continental rift-
610 related magmatism on the northeast Canadian Arctic margin. German Journal Geosciences,
611 164 (1), 107-130.
612 Evenchick, C.A., Davis, W.J., Bédard, J.H., Hayward, N., Friedman, R.M., 2015. Evidence for
613 protracted high Arctic large igneous province magmatism in the central Sverdrup Basin from
614 stratigraphy, geochronology, and paleodepths of saucer-shaped sills. GSA Bulletin, DOI:
615 10.1130/B31190.1.
616 Forster, A., Schouten, S., Moriya, K., Wilson, P.A., Sinninghe Damsté, J.S., 2007. Tropical
617 warming and intermittent cooling during the Cenomanian/Turonian oceanic anoxic event 2:
618 Sea surface temperature records from the equatorial Atlantic. Paleoceanography, 22,
619 PA1219, DOI:10.1029/2006PA001349.
620 Friedrich, O., Norris, R.D., Erbacher, J., 2012. Evolution of middle to Late Cretaceous oceans –
621 A 55 m.y. record of Earth's temperature and carbon cycle. Geology, DOI:10.1130/G32701.1.
622 Galloway, J.M., Sweet, A.R., Pugh, A., Schröder-Adams, C.J., Swindles, G.T., Haggart, J.W.,
623 Embry, A.F., 2012. Correlating middle Cretaceous palynological records from the Canadian
624 High Arctic based on a section from the Sverdrup Basin and samples from the Eclipse
625 Trough. Palynology, 36:2, 277-302.
626 German, C.R., von Damm, K.L., 2006. Hydrothermal processes. In Elderfield, H. (ed.), The
627 Ocean and marine Geochemistry. Treatise on Geochemistry, Volume 6, 181-222. Elsevier.

628 Gooday, A.J., Bernhard, J.M., Levin, L.A., Suhr, S., 2000. Foraminifera in the Arabian Sea
629 OMZ and other oxygen deficient settings: taxonomic composition, diversity and relation
630 to metazoan faunas. Deep-Sea Research II, 47, 25–54. DOI:10.1016/S0967-0645(99)00099-
631 5.
632 Gradstein, F.M., Ogg, J.G., Schmitz, M.D., Ogg, G.M., 2012. The Geologic Time Scale 2012,
633 Volume 2: Oxford, United Kingdom, Elsevier, 1144 p.
634 Helz, G.R., Miller, C.V., Charnock, J.M., Mosselmans, J.F.W.,
635 Pattrick, R.A.D., Garner, C.D., and Vaughan, D.J., 1996.
636 Mechanism of molybdenum removal from the sea and its
637 concentration in black shales: EXAFS evidence: Geochimica et
638 Cosmochimica Acta, 60, 3631–3642, DOI:10.1016/0016-
639 7037(96)00195-0.
640 Herrle, J.O., Pross, J., Friedrich, O., Hemleben, C., 2003. Short-term environmental changes in
641 the Cretaceous Tethyan Ocean: Micropaleontological evidence from the Early Albian
642 Oceanic Anoxic Event 1b. Terra Nova, 15, 14-19.
643 Herrle, J.O., Schröder-Adams, C.J., Davis, W., Pugh, A.T., Galloway, J.M., Fath, J., 2015. Mid-
644 Cretaceous High Arctic stratigraphy, climate, and Oceanic Anoxic Events. Geology, 43, 403-
645 406.
646 Holmden, C., Jacobson, A.D., Sageman, B.B., Hurtgen, M.T., 2016, Response of the Cr isotope
647 proxy to Cretaceous Anoxic Event 2 in a pelagic carbonate succession from the Western
648 Interior Seaway. Geochimica et Cosmochimica Acta, 186, 277-295.
649 Jaffe, A.L., Peucker-Ehrenbrink, B., Petsch, S.T., 2002. Mobility of rhenium, platinum group
650 elements and organic carbon during black shale weathering. Earth and Planetary Science
651 Letters, 198. 339-353.

652 Jarvis, I., Gale, A.S., Jenkyns, H.C., Pearce, M.A., 2006. Secular variation in the late Cretaceous
653 carbon isotopes: a new $\delta^{13}C$ carbonate reference curve for the Cenomanian–
654 Campanian (99.6–70.6 Ma). Geological Magazine 143, 561–608.
655 Jenkyns, H.C., Dickson, A.J., Ruhl, M., Van Den Boorn, S.H.J.M., 2017. Basalt-seawater
656 interaction, the Plenus Cold Event, enhanced weathering and geochemical change:
657 deconstructing Oceanic Anoxic Event 2 (Cenomanian-Turonian, Late Cretaceous).
658 Sedimentology, 64, 16-43.
659 Joo, Y.J., Sageman, B.B., 2014. Cenomanian to Campanian carbon isotope chemostratigraphy
660 from the Western Interior Basin, U.S.A. Journal of Sedimentary Research, 84, 529-542.
661 Jorissen, F.J., de Stigter, H.C., Widmark, J.G.V., 1995. A conceptual model explaining benthic
662 foraminiferal microhabitats. Marine Micropaleontology, 22, 3–15. DOI:10.
663 1016/0377-8398(95)00047-X.
664 Jowitt, S.M., Williamson, M., Ernst, R.E., 2014. Geochemistry of the 130 to 80 Ma Canadian
665 Arctic Large Igneous province (HALIP) event and implications for Ni-Cu-PGE
666 prospectivity. Economic Geology, 109, 281-307.
667 Kingsbury, C. G., Kamo, S. L., Ernst, R. E., Söderlund, U., Cousens, B. L., 2018. U-Pb
668 geochronology of the plumbing system associated with the Late Cretaceous Strand Fiord
669 Formation, Axel Heiberg Island, Canada: part of the 130-90 Ma High Arctic large igneous
670 province. Journal of Geodynamics DOI: 10.1016/j.jog.2017.11.001.
671 Kuhnt, W., A.E. Holbourn, S. Beil, M. Aquit, T. Krawczyk, S. Flogel, E.H. Chellai, H. Jabour,
672 2017, Unravelling the onset of Cretaceous Oceanic Anoxic Event 2 in an extended sediment
673 archive from the Tarfaya-Laayoune Basin, Morocco, Paleoceanography, DOI:
674 10.1002/2017PA003146.

675 Lenniger, M., Nøhr-Hansen, H., Hills, L.V., Bjerrum, C.J., 2014, Arctic black shale
676 formation during Cretaceous Oceanic Anoxic Event 2. Geology 42, 799-802.
677 Liao, S., Tao, C., Li, H., Zhang, G., Liang, J., Yang, W., Wang, Y., 2018. Surface sediment
678 geochemistry and hydrothermal activity indicators in the Dragon Horn area on the Southwest
679 Indian Ridge. Marine Geology, 398, 22-34.
680 MacRae, R.A., 1992. Palynology of the Bastion Ridge and Strand Fiord formations, western
681 Axel Heiberg Island. Canadian Arctic Islands, N.W.T.: implications for stratigraphy, age,
682 paleoenvironment, and *Nyktericysta* taxonomy. M.Sc. thesis, University of Calgary, Alberta.
683 347 p.
684 MacRae, R.A., Hills, L.V., McIntyre, D.J., 1996. The paleoecological significance of new
685 species of *Limbicysta* (Acritarcha) from the upper Albian of the Canadian Arctic islands.
686 Canadian Journal of Earth Sciences, 33, 1475-1486.
687 Mao, S., Wan, C., Qiao, X., 1999. Cretaceous nonmarine dinoflagellates from northeast China.
688 Grana, 38, 144-161.
689 Meyers, S.R., Siewert, S.E., Singer, B.S., Sageman, B.B., Condon, D.J., Obradovich, J.D., Jicha,
690 B.R., Sawyer, D.A., 2012. Intercalibration of radioisotopic and astrochronologic time scales
691 for the Cenomanian-Turonian boundary interval, Western Interior Basin, USA. Geology, 40
692 (1), 7-10.
693 Murray, J.W., Alve, E., Jones, B.W., 2011. A new look at modern agglutinated benthic
694 foraminiferal morphogroups: their value in palaeoecological interpretation. Palaeogeography,
695 Palaeoclimatology, Palaeoecology, 309, 229-241.
696 Mudie, P.J., 1982. Pollen distribution in recent marine sediments, eastern Canada. Canadian
697 Journal of Earth Sciences, 19, 729-747.

698 Nagy, J., 1992. Environmental significance of foraminiferal morphogroups in Jurassic North Sea
699 deltas: Palaeogeography, Palaeoclimatology, Palaeoecology, 95, 111-134.
700 Núñez-Betelu, L.K., MacRae, R.A., Hills, L.V., Muecke, G.K., 1994. Uppermost Albian
701 Campanian palynological biostratigraphy of Axel Heiberg and Ellesmere islands
702 (Canadian Arctic). In: Thurston, D.K., Fujita, K. (eds.), Proceedings of the 1992 International
703 Conference on Arctic Margins, Anchorage, Alaska. U.S. Department of the
704 Interior, Anchorage, Alaska, p. 135–140.
705 Paul, C.R.C., Mitchell, S.F., Marshall, J.D., Leary, P.N., Gale, A.S., Duane, A.M., Ditchfield,
706 P.W., 1994. Palaeoceanographic events in the Middle Cenomanian of Northwest Europe.
707 Cretaceous Research 15, 707–738.
708 Pratt, L.M., Kauffman, E.G., Zelt, F.B., 1985. Fine-grained deposits and biofacies of the
709 Cretaceous Western Interior Seaway: Evidence for cyclic sedimentary processes. Society
710 Economic Paleontology, Mineralogy Fieldtrip Guidebook 4, 1985 Midyear Meeting, Golden,
711 Colorado.
712 Pugh, A.T., Schröder-Adams, C.J., Carter, E.S., Herrle, J.O., Galloway, J., Haggart, J.W.,
713 Andrews, J.L., Hatsukano, K., 2014. Cenomanian to Santonian radiolarian biostratigraphy,
714 carbon isotope stratigraphy and paleoenvironments of the Sverdrup Basin, Ellef Ringnes
715 Island, Nunavut, Canada. Palaeogeography, Palaeoclimatology, Palaeoecology, 413, 101-
716 122.
717 Quesnel, A., Schröder-Adams, C.J., Davies, W., 2017. Cretaceous (Albian to Cenomanian)
718 biostratigraphic, paleogeographic and paleoenvironmental reconstruction of the northern
719 Western Interior Sea: Yukon, Canada. Palaeogeography, Palaeoclimatology, Palaeoecology,
720 468, 453-472.

721 Reolid, M., Nikitenko, B.L., Glinskikh, L., 2014. *Trochammina* as opportunist foraminifera in
722 the Lower Jurassic from north Siberia. Polar Research, 33:1, DOI:10.3402/polar.v33.21653.
723 Ricketts, B., Osadetz, K.G., Embry, A.F., 1985. Volcanic style in the Strand Fiord Formation
724 (Upper Cretaceous), Axel Heiberg Island, Canadian Arctic Archipelago. Polar Research, 3,
725 107-122.
726 Ross, J.B., Ludvigson, G.A., Schröder-Adams, C.J., and Suarez, M.B., in press. High latitude
727 meteoric $\delta^{18}O$ compositions from the Cenomanian Bastion Ridge Formation, Axel Heiberg
728 Island, Canadian Arctic Archipelago: A paleoclimate proxy from the Sverdrup
729 Basin. In Wagreich. M., (ed.), Cretaceous Climate Events and Short-Term Sea-Level
730 Changes, Geological Society London, Special Publication.
731 Saumur, B.M., Dewing, K., Williamson, M.-C., 2016. Architecture of the Canadian portion of
732 the High Arctic Large Igneous Province and implications for magmatic Ni-Cu potential.
733 Canadian Journal of Earth Sciences, 53, 528-542.
734 Scaife, J.D., Ruhl., M., Dickson, A.J., Mather, T.A., Jenkyns, H.C., Percival, L.M.E., Hesselbo,
735 S.P., Cartwright, J., Eldrett, J.S., Bergman, S.C., Minisini, D. Sedimentary mercury
736 enrichments as a marker for submarine Large Igneous Province volcanism? Evidence from
737 the Mid-Cenomanian Event and Oceanic Anoxic Event 2. Geochemistry, Geophysics,
738 Geosystems, 18, 4253-4275.
739 Schröder-Adams, C.J., Herrle, J.O., Embry, A.F., Haggart, J.W., Galloway, J.M., Pugh, A.T.,
740 Harwood, D.M., 2014. Aptian to Santonian foraminiferal biostratigraphy and
741 paleoenvironmental change in the Sverdrup Basin as revealed at Glacier Fiord, Axel Heiberg
742 Island, Canadian Arctic Archipelago. Palaeogeography, Palaeoclimatology, Palaeoecology,
743 413, 81-100.

744 Sheta, A.S., Falatah, A.M., Al-Sewailem, M.S., Khaled, E.M., Sallam, A.S.H., 2003. Sorption
745 characteristics of zinc and iron by natural zeolite and bentonite. Microporous and
746 mesoporous Materials, 61, 127-136.
747 Sinninghe Damsté, J.S., van Bentum, E.C., Reichert, G.-J., Pross, J., Schouten, S., 2010. A CO_2
748 decrease-driven cooling and increased latitudinal temperature gradient during the mid
749 Cretaceous Oceanic Anoxic Event 2. Earth and Planetary Science Letters, DOI:
750 10.1016/j.epsl.2010.02.027.
751 Snow, L.J., Duncan, R.A., Bralower, T.J., 2005. Trace element abundances in the Rock
752 Canyon Anticline, Pueblo, Colorado, marine sedimentary section and their relationship
753 to Caribbean plateau construction and oxygen anoxic event 2. Paleoceanography
754 20, PA3005. DOI: 10.1029/2004PA001093.
755 Souther, J.G., 1963. Geological traverse across Axel Heiberg Island from Buchanan Lake to
756 Strand Fiord. Geological Survey of Canada, Memoir 320, 426-448.
757 Svensen, H., Planke, S., Polozov, A.G., Schmidbauer, N., Corfu, F., Podladchikov, Y.Y.,
758 Jamtveit, B., 2009. Siberian gas venting and the end-Permian environmental crisis. Earth and
759 Planetary Science Letters, 277, 490-500.
760 Svensen, H., Planke, S., Malthe-Sørenssen, A., Jamtveit, B., Myklebust, R., Rasmussen Eidem,
761 T., Rey, S.S., 2004. Release of methane from a volcanic basin as a mechanism for initial
762 Eocene global warming. Nature, 429, 542-545.
763 Tarduno, J.A., Brinkman, D.B., Renne, P.R., Cottrell, R.D., Scher, H., Castillo, P., 1998.
764 Evidence for extreme climatic warmth from Late Cretaceous Arctic vertebrates. Science,
765 282, 2241–2244.

766 Tegner, C., Storey, M., Holm, P.M., Thorarinsson, S.B., Zhao, X., Lo, C.-H., Knudsen, M.F.,
767 2011. Magmatism and Eurekan deformation in the High Arctic Large Igneous Province:
768 ^{40}Ar-^{39}Ar age of Kap Washington Group volcanics, North Greenland. Earth and Planetary
769 Science Letters, 303, 203-214.
770 Thorarinsson, S.B., Holm, P.M., Tapper, S., Heaman, l.M., Tegner, C., 2011. Late Cretaceous-
771 Palaeocene continental rifting in the High Arctic: U-Pb geochronology of the Kap
772 Washington Group volcanic sequence, North Greenland. Journal of the Geological Society,
773 London, 168, 1093-1106.
774 Thorsteinsson, R, 1971. Geology, Strand Fiord. Geological Survey of Canada Map 1301A.
775 Tsikos, H., Jenkyns, H.C., Walsworth-Bell, B., Petrizzo, M.R., Forster, A., Kolonic, S., Erba, E.,
776 Premoli-Siva, I.P., Baas, M., Wagner, T., Sinninghe Damsté, J.S., 2004. Carbon-isotope
777 stratigraphy recorded by the Cenomanian-Turonian Oceanic Anoxic Event: correlation and
778 implications based on three key localities. Memoir Geological Society of London, 161, 711-
779 719.
780 Turgeon, S.C., Creaser, R.A., 2008. Cretaceous Anoxic Event 2 triggered by a massive magmatic
781 episode. Nature, 454, 323-326.
782 Van Helmond, N.A.G.M., Sluijs, A., Reichart, G.-J., Sinninghe Damsté, J.S., Slomp, C.P.,
783 Brinkhuis, H., 2013. A perturbed hydrological cycle during Oceanic Anoxic Event 2.
784 Geology, DOI: 10.1130/G34929.1.
785 Villeneuve, M., Williamson, M.-C. 2006. ^{40}Ar-^{39}Ar dating of mafic magmatism from the
786 Sverdrup Basin Magmatic Province. In Scott, R.A., Thurston D.K. (eds.). Proceedings of the
787 4th Int. Conf. on Arctic Margins (ICAM IV), 206–215, Anchorage Alaska. (OCS Study,
788 MMS 2006-003, U.S. Department of the Interior).

789 Wagner T., Magill C.R., Herrle J.O., 2018. Carbon Isotopes. In: White W. (eds.)
790 Encyclopedia of Geochemistry. Encyclopedia of Earth Sciences Series. Springer, Cham.

791 Williamson, M.-C., 1988. The Cretaceous igneous province of the Sverdrup Basin, Canadian
792 Arctic: Field relations and petrochemical studies. Ph.D. thesis, Dalhousie University,
793 Halifax, Nova Scotia. 417 p.

794 Williamson, M.-C., 2016. Report of Activities for High Arctic large Igneous Province (HALIP) –
795 GEM 2 Western Arctic Region project: Bedrock Mapping and Mineral Exploration.
796 Geological Survey of Canada Open File 7950, 48 p.

797 Wohlwend, S., Hart, M., Weissert, H., 2016. Chemostratigraphy of the Upper Albian to mid-
798 Turonian Natih Formation (Oman) – how authigenic carbonate changes a global pattern. The
799 Depositional Record, DOI: 10.1002/dep2.15.

800 Zhang, X., Chen, K., Hu, D., Sha, J., 2016. Mid-Cretaceous carbon cycle perturbations and
801 Oceanic Anoxic Events recorded in southern Tibet. Scientific Reports, 6, 39643, DOI:
802 10.1038/srep39643.

803 Zheng, X.-Y., Jenkyns, H.C., Gale, A.S., Ward, D.J., Henderson, G.M., 2013. Changing
804 ocean circulation and hydrothermal inputs during Oceanic Anoxic Event 2
805 (Cenomanian–Turonian): Evidence from Nd-isotopes in the European shelf sea.
806 Earth Planetary Science Letters. DOI: 10.1016/j.epsl.2013.05.053i.

807

808 **Figure Captions**

809 Figure 1: A) Locality map of Queen Elizabeth Islands, Canadian High Arctic. B) Map of Axel
810 Heiberg Island. Star indicates section locality at head of Glacier Fiord. The circled area shows

811 the approximate extent of the Strand Fiord Formation on Axel Heiberg Island (after Estrada and
812 Henjes-Kunst, 2013).

813 Figure 2: Stratigraphic framework of the upper Albian to Campanian interval based on sections
814 on Ellef Ringnes Island representing the basin centre (Pugh et al., 2014), Bunde Fiord and Strand
815 Fiord as the main localities of the Strand Fiord volcanics (Rickett et al., 1985, MacRae et al.,
816 1996), Glacier Fiord (Schröder-Adams et al., 2014 and this study) and Slidre Fiord, a marginal
817 basin position (Davies et al., 2018). The stratigraphic position of OAE2 as a timeline is known
818 from Slidre Fiord (Davies et al., 2018), Glacier Fiord (Herrle et al., 2015 and this study) and
819 Hoodoo Dome (Pugh et al., 2014). The presence of the OAE2 interval at Strand Fiord is
820 unknown. Bunde Fiord shows the thickest extent of Strand Fiord Formation, but no Kanguk
821 Formation is exposed (for localities see Fig. 1B). The age of the Kanguk transgression in these
822 localities is questionable. Note the diachronous basal boundary of the Kangak Formation.
823 Canada Basin Events after Embry and Osadetz (1988). Age of Wootton Intrusive Complex on
824 Ellesmere Island after Estrada and Henjes-Kunst (2013).

825 Figure 3: A) Measured and analyzed section at Glacier Fiord (red line). Arrow points toward the
826 sequence boundary at the Albian/Cenomanian Boundary at the base of the Bastion Ridge
827 Formation expressed as a thin paleosol. A second sequence boundary is expressed by freshwater
828 siderite beds within the upper Bastion Ridge Formation of middle Cenomanian age. The OAE2
829 interval in the lower Kanguk Formation is marked. The interval immediately above the upper
830 sandstone unit of the Bastion Ridge Formation is not well exposed on that side of the glacial
831 stream that flows in front of the section. In 2014 it was measured on the opposite stream cut, not
832 shown here. B) View from Lost Hammer Diapir of the Hassel Formation overlain by the flood
833 basalts of the Strand Fiord Formation north of Glacier Fiord. The regionally restricted Bastion

Ridge Formation is not exposed here. C) Close-up of middle Bastion Ridge Formation showing the iron-rich sediments of the restricted basin, particularly in the upper half. A bioturbated shoreface sandstone forms the ridge. D) Contact between the Strand Fiord volcanics and the Kanguk Formation at Expedition Fiord (photo courtesy of Simon Schneider).

Figure 4: Measured section at Glacier Fiord after Schröder-Adams et al. (2014) with additional resampling from 2014 field season; bentonite ages after Davis et al. (2016). The response to magmatic events is shown through Os_i (94), ^{192}Os and Re curves; the data of these parameters of both field seasons were complementary, but not overlapping. These are plotted against $\delta^{13}C_{org}$ and TOC (%) content. Note the marked time interval of the last Strand Fiord volcanic pulse. Elevated Zn/Al and Mn/Al and Fe values point towards hydrothermal activity. Note the different scales in the Zn/Al scale for the 2011 samples (blue) and 2014 samples (black). The iron increase within the Bastion Ridge Formation can be seen on Figure 3C. Age levels are marked by letters, of which A to F are calculated by sedimentation rates according to Davis et al. (2016). The commonly used age levels of A, B and C for the OAE2 interval are adopted here and ages established for the Yezo Group, Japan (duVivier et al., 2015) are listed for comparison.

Figure 5: Ratios of TOC (%) over S (%) throughout the section. Note the elevated ratios due to lower concentrations of dissolved sulfate in the brackish to freshwater/terrestrial Bastion Ridge Formation with the exception of the basal interval that delivered benthic foraminifera. Marine values mark the Kanguk Formation.

Figure 6: Paleoenvironmental changes over the Cenomanian/Turonian boundary interval at Glacier Fiord. Proxies utilized here include lithology, presence/absence and abundances of benthic foraminifera, their morphotype dominance, $\partial^{13}C_{org}$, TOC (%) content, Hydrogen Index

and Os_i variation. In addition, marine (blue) versus brackish/freshwater (grey) intervals are marked.

Figure 1

Click here to download Figure: Figure 1.pdf

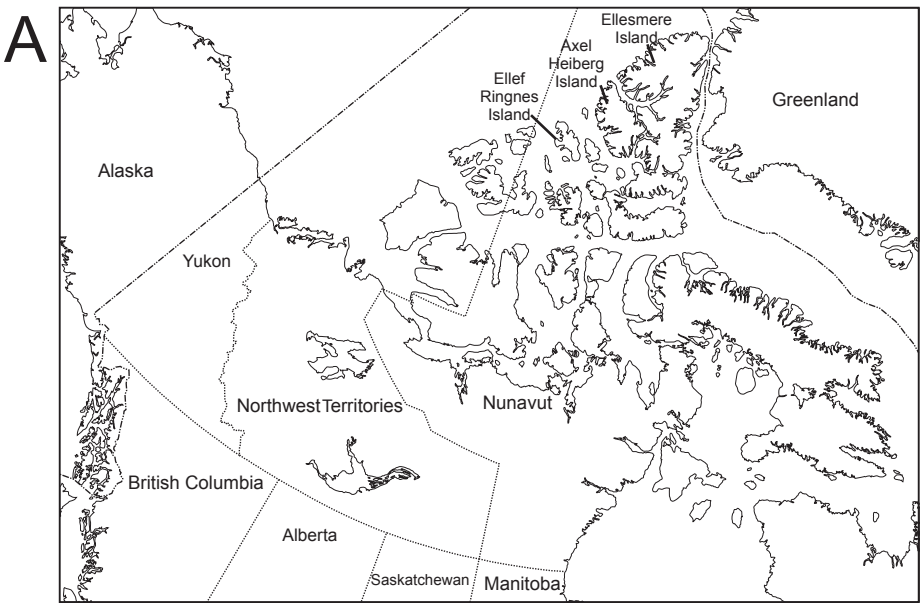

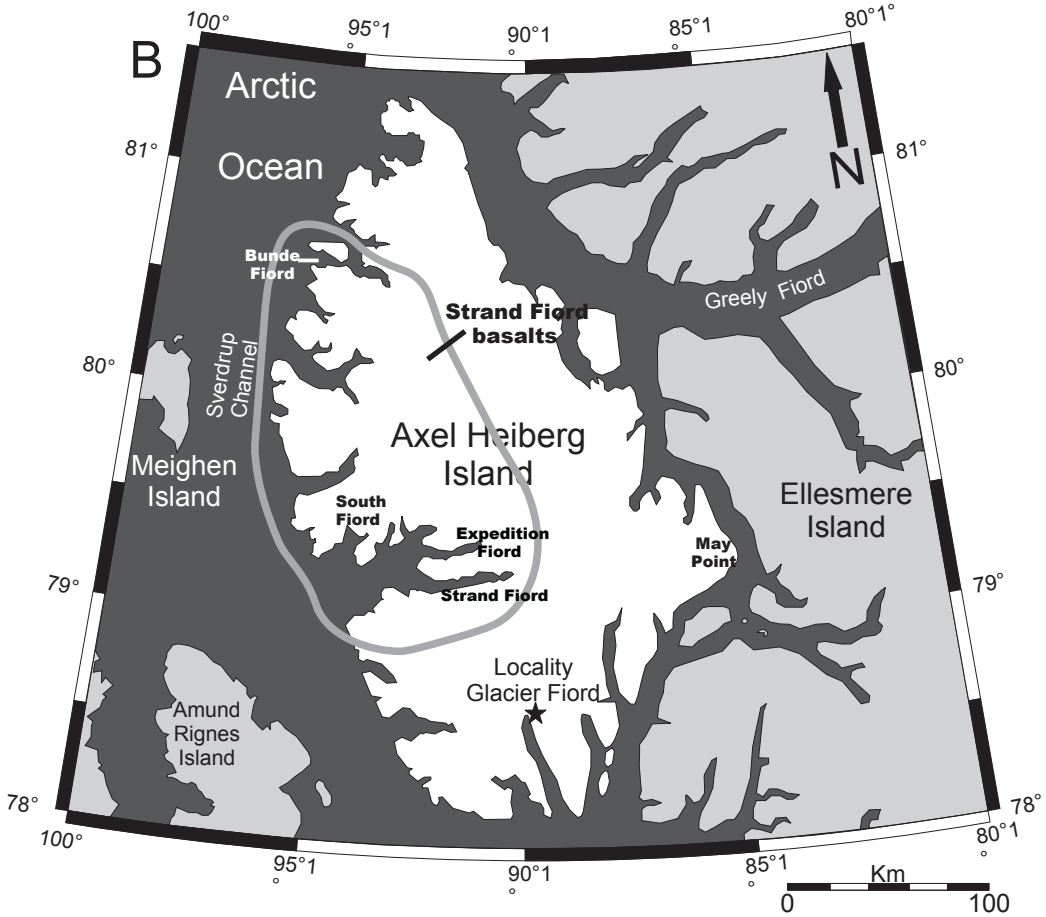

Figure 2

Click here to download Figure: Figure 2.pdf

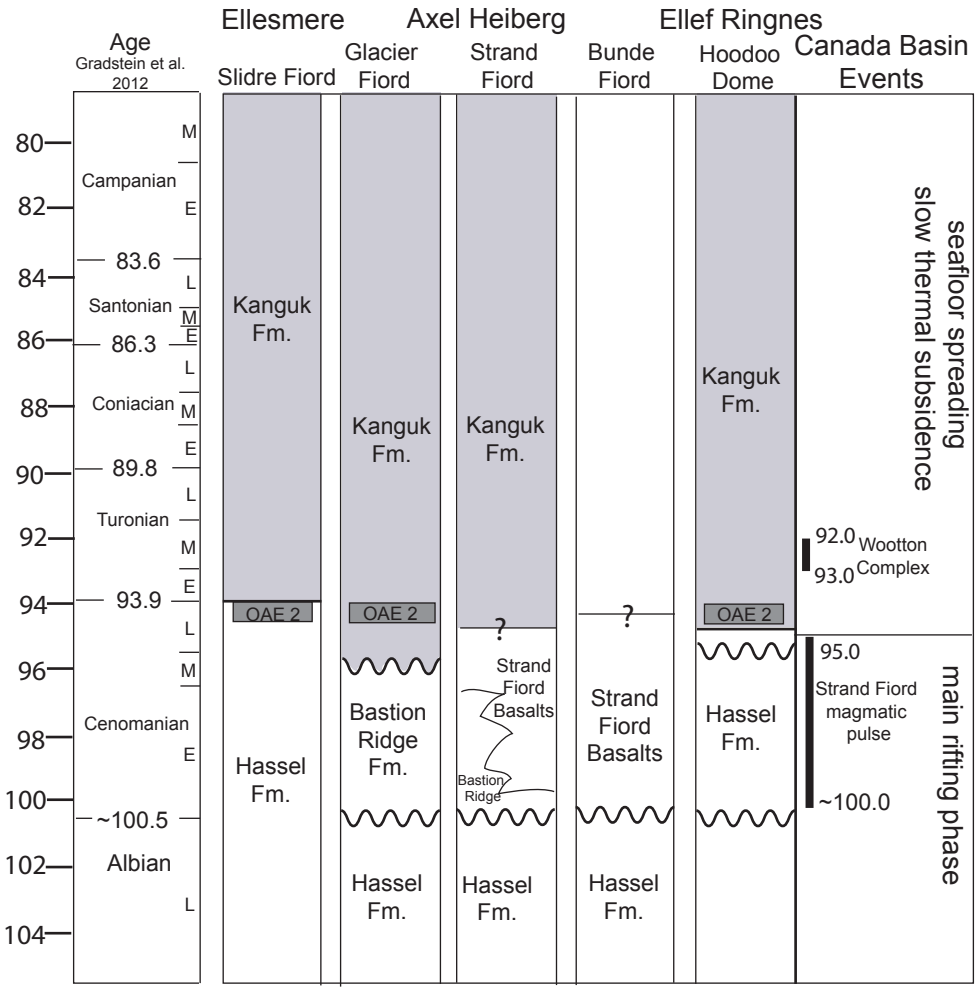

Figure 3

Click here to download high resolution image

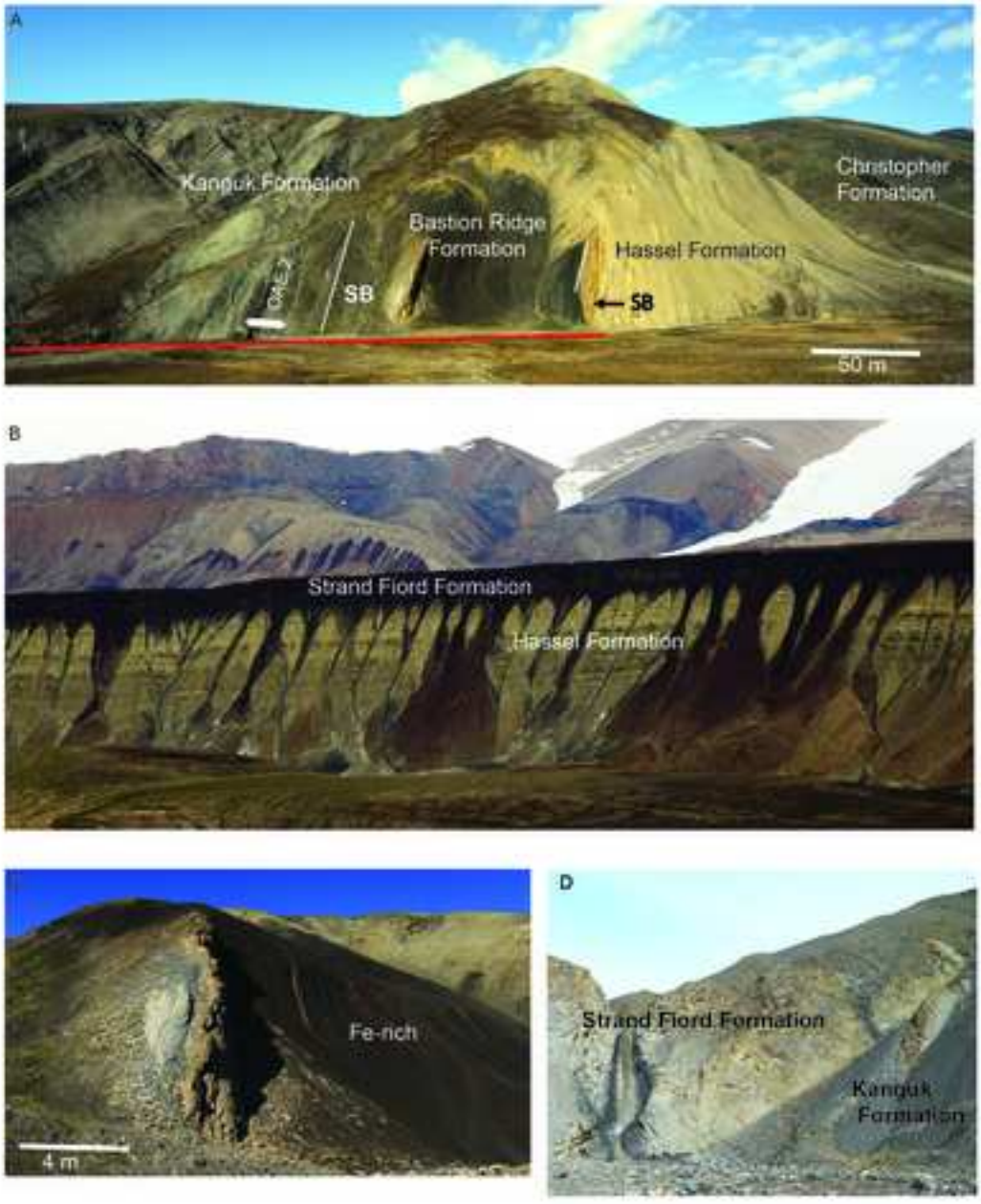

Figure 4

Click here to download Figure: Figure 4.pdf

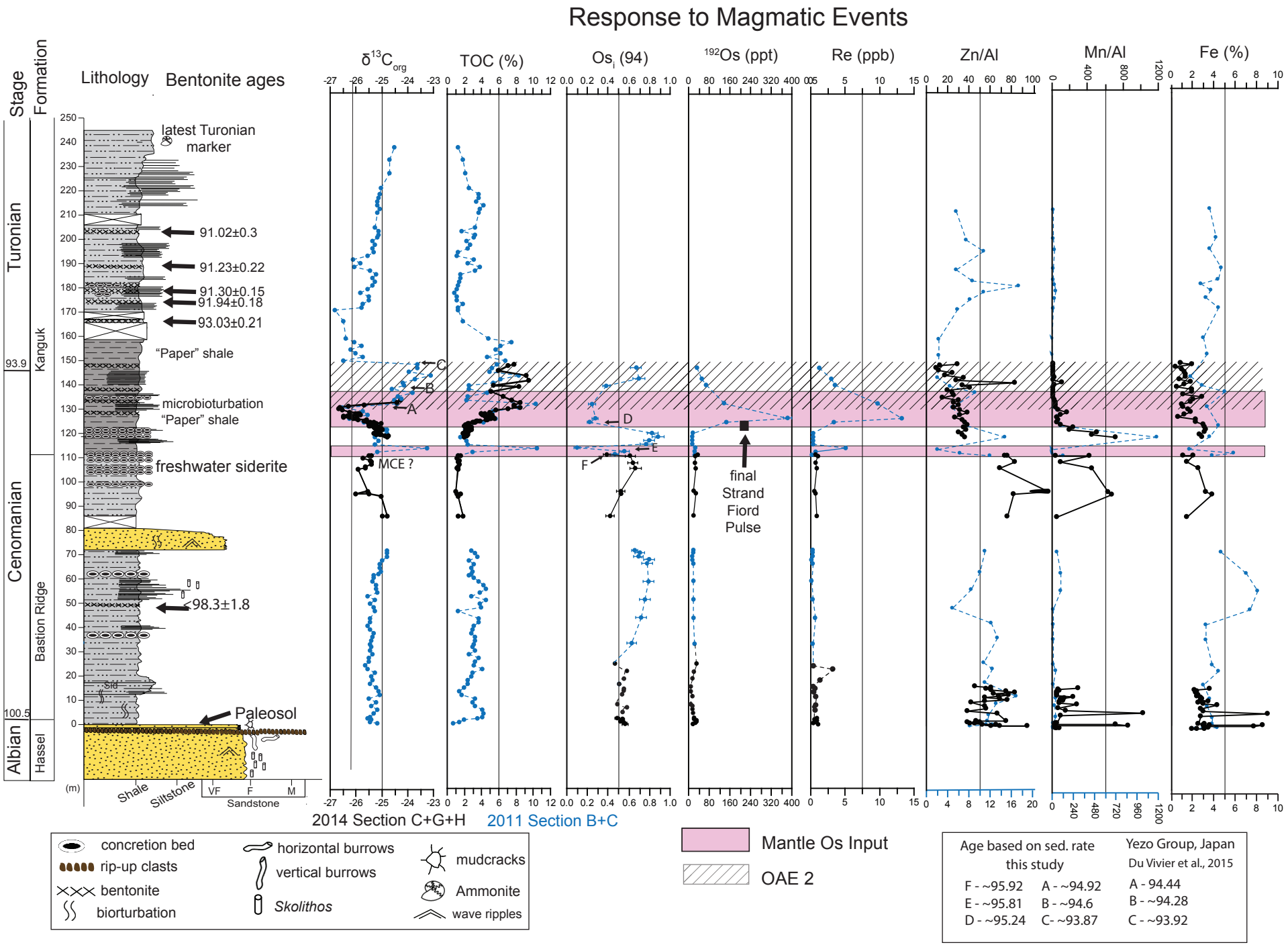

Figure 5

Click here to download Figure: Figure 5.pdf

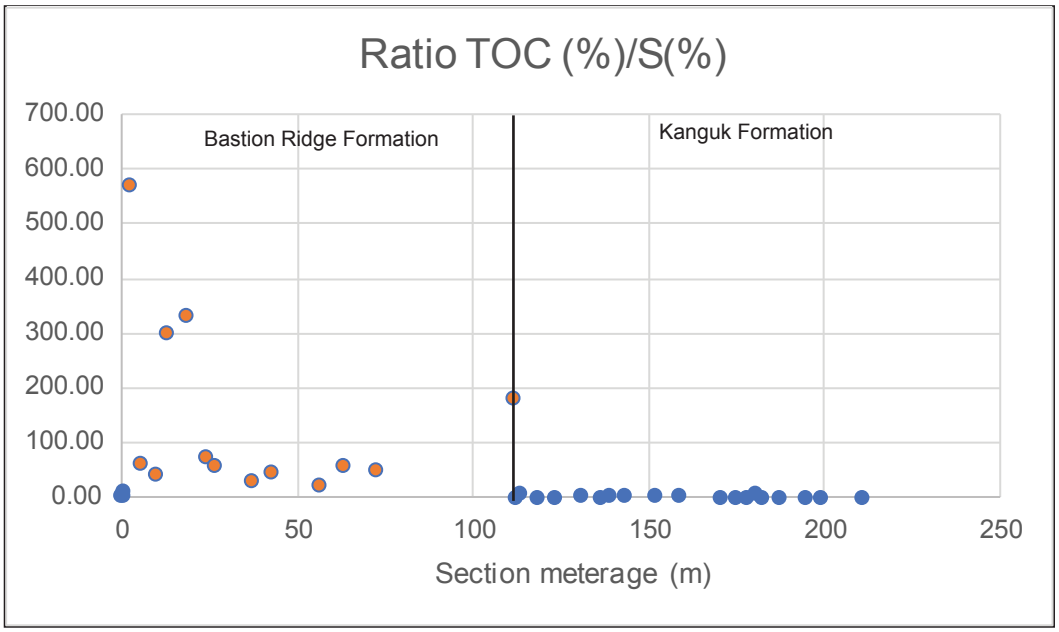

Figure 6

Click here to download Figure: Figure 6.pdf

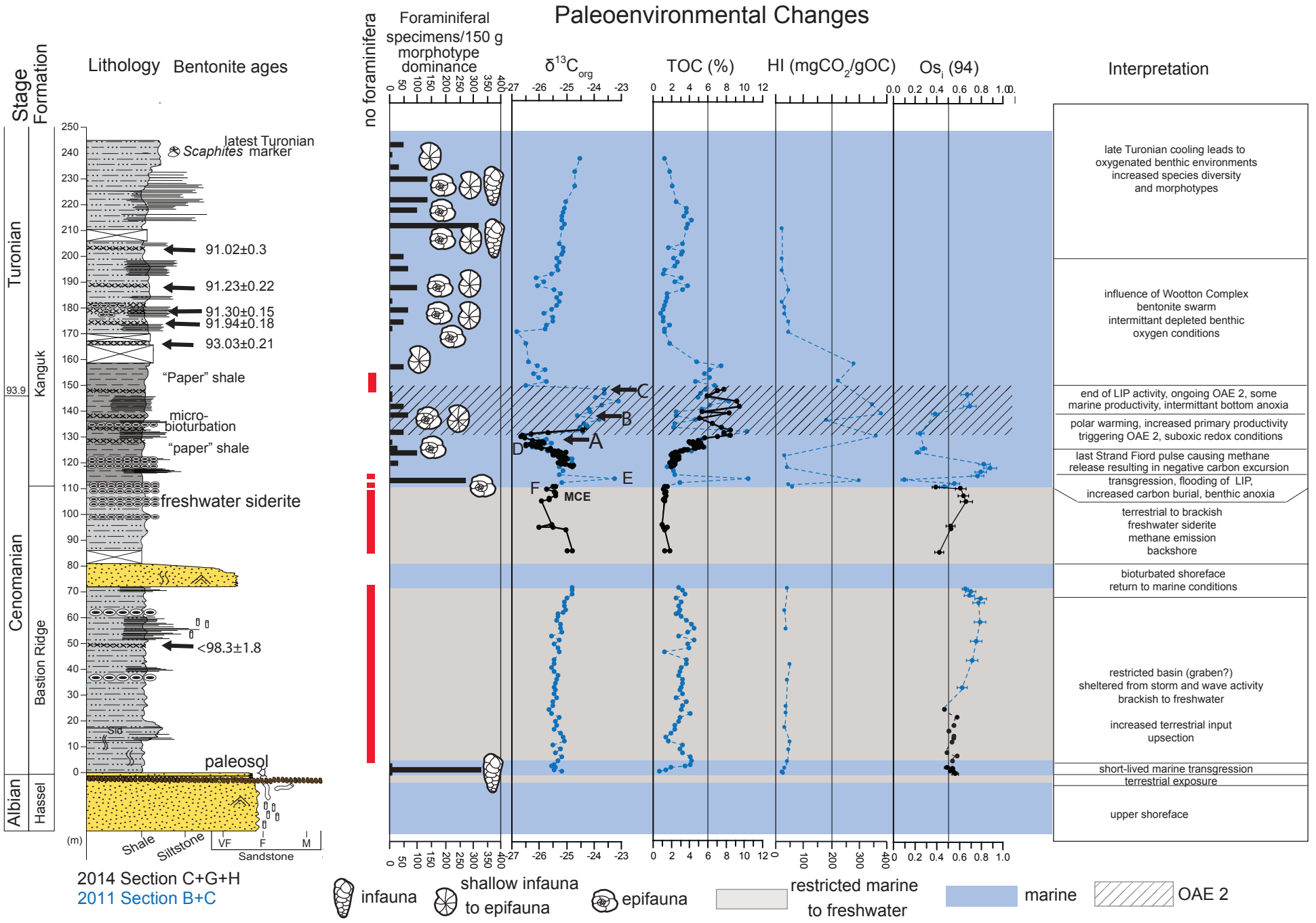

Supplementary material for online publication only Methods

Click here to download Supplementary material for online publication only: Methods for Supplementary Material.docx

Supplementary material for online publication only Table 1

Click here to download Supplementary material for online publication only: Table 1.xlsx

Supplementary material for online publication only Table 2

Click here to download Supplementary material for online publication only: Table 2.xlsx

Supplementary material for online publication only Table 3

Click here to download Supplementary material for online publication only: Table 3.xlsx